Renewable and Sustainable Energy Reviews 161 (2022) 112286

Contents lists available at ScienceDirect

Renewable and Sustainable Energy Reviews

journal homepage: www.elsevier.com/locate/rser

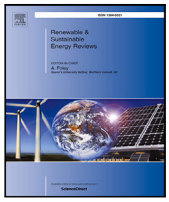

Sizing and optimization process of hybrid electric propulsion system for heavy-duty vehicle based on Gaussian process modeling considering traction motor characteristics

Dong-Min Kim [a], Soo-Gyung Lee [b], Dae-Kee Kim [c], Min-Ro Park [d], Myung-Seop Lim [c,*]

[a] Department of Automotive Engineering, Honam University, Gwangju, 62399, Republic of Korea
[b] Material Performance Research Group, POSCO Global R&D Center, Incheon, 21985, Republic of Korea
[c] Department of Automotive Engineering, Hanyang University, Seoul, 04763, Republic of Korea
[d] Department of Electrical Engineering, Soonchunhyang University, Asan, 31538, Republic of Korea

ARTICLE INFO

Keywords:
Component sizing
Equivalent circuit
Fuel economy optimization
Gaussian process modeling (GPM)
Hybrid electric propulsion system

ABSTRACT

This paper suggests a sizing and optimization scheme of a hybrid electric propulsion system for a heavy-duty vehicle. The considered propulsion system consists of four in-wheel traction motors with a planetary gear, and the power source is configured with a battery and engine–generator set. To optimize fuel economy by powertrain sizing, the vehicle design process and vehicle simulation were constructed. Optimization was then performed using Gaussian process modeling (GPM). During the optimization, the variation of the gross weight of the propulsion system was considered. In addition, the change in the efficiency map of the traction motor was precisely reflected. The sampling points for GPM were determined from the Optimal Latin hypercube design. Subsequently, the fuel economy surrogate model was generated via the GPM. Optimization was then performed using the steepest gradient descent algorithm. Finally, the maximized fuel economy model was verified using a vehicle simulation.

1. Introduction

As the problem of air pollution gradually worsens, heavy-duty diesel vehicles have received significant attention as the primary cause of air pollution globally [1,2]. As a result, research on the electrification of heavy-duty vehicles are actively being conducted. However, it is not clear whether a battery-only electric vehicle is appropriate scheme for heavy-duty applications. Problems regarding the weight of the battery and its charging time exist as well [3–5]. Although studies are being conducted on the energy density and charging speed of batteries, it is difficult to reduce the burden from battery weight on heavy-duty vehicles over a short duration [6]. In this situation, a hybrid electric vehicle (HEV) could be used as an alternative solution [7].

Significant amounts of numerical and experimental research on vehicle hybridization are available in literature. A majority of the reported studies have focused on passenger and commercial vehicles. Recently, vehicle hybridization types and topics of research have become more varied. Gu et al. developed a multi-mode hybrid powertrain system with two planetary gear by using integrated optimization technique [8]. Cammalleri et al. investigated transmission for hybrid vehicle considering the number of modes and planetary gearing [9]. In terms of heavy-duty applications, Liu et al. developed an energy management strategy based on reinforcement learning for a parallel hybrid electric truck and Mamun et al. investigated the implementation method for a supercapacitor equipped series hybrid electric military vehicle [10,11]. Not limited to the ground vehicles, Khan et al. researched fuzzy logic based energy management of all electric ship [12]. Furthermore, study on control strategy considering battery characteristics by using signal injection in HEV has also been conducted [13]. Lately, distributed and double deep learning based energy management of HEV were also suggested [14,15].

In the research on HEVs, there exist two problems in the sizing of the propulsion systems. One problem is the gear ratio determination for the electric powertrain, and the other is the distribution of the power between the battery and engine–generator set. In the textbook, the gear ratio was designed based on the predetermined traction motor speed, wheel radius, and maximum vehicle speed. Furthermore, the engine–generator specification was determined to meet the required power of the vehicle at a regular highway speed on a flat road [16]. However, the component sizing is crucial to vehicle design [17]. Therefore, there were many studies on component sizing. In Table 1, studies

* Corresponding author.
E-mail address: myungseop@hanyang.ac.kr (M.-S. Lim).

https://doi.org/10.1016/j.rser.2022.112286
Received 18 September 2021; Received in revised form 10 December 2021; Accepted 15 February 2022
Available online 9 March 2022

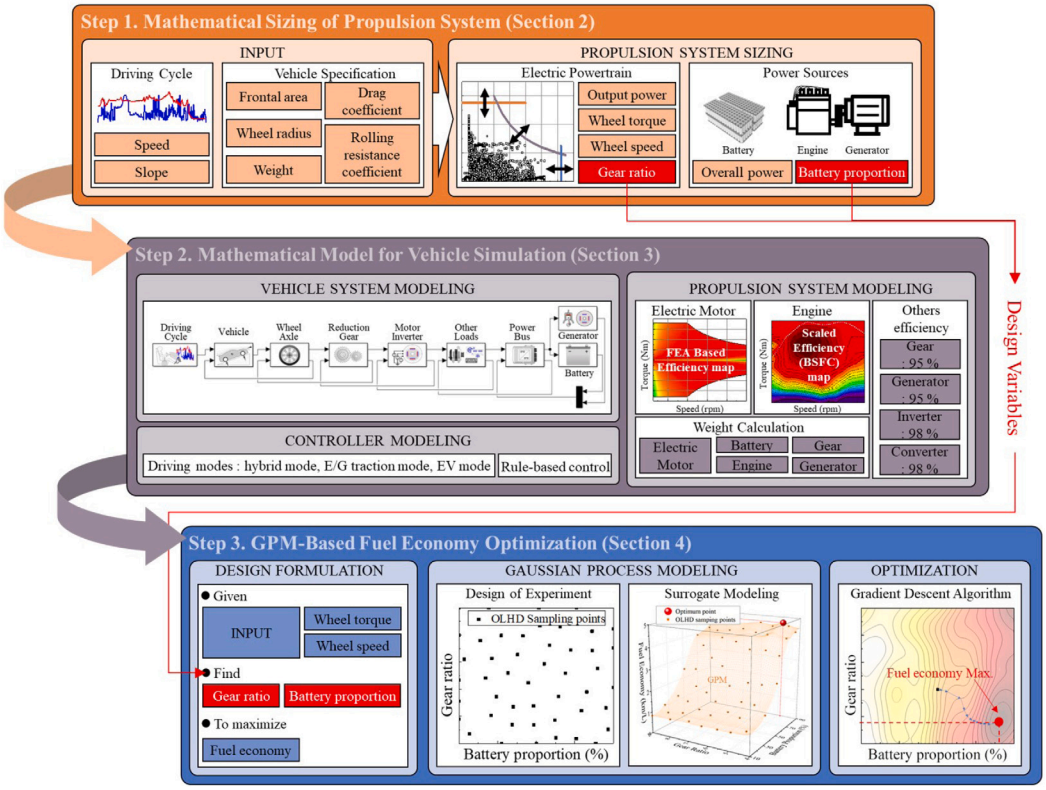

Fig. 1. Suggested sizing and optimization process for hybrid electric vehicle.

Table 1
Recent studies on component sizing of hybrid electric vehicles.

Sizing component	Type	Year	Ref.
Battery, fuel cell	FCEV	In press	[18]
Battery, electric motor, engine	HEV	2021	[19]
Battery, ultra-capacitor	HESSEV	2021	[20]
Battery, fuel cell, engine	HEV	2021	[21]
Battery	HEV	2021	[22]
Battery, electric motor, engine	HEV	2021	[23]
Battery, super-capacitor	HESSEV	2021	[24]
Battery, super-capacitor	HESSEV	2021	[25]
Battery, electric motor, gear ratio	HEV	2021	[26]
Battery, fuel cell, fuel tank	FCEV	2021	[27]
Battery, super-capacitor	HESSEV	2020	[28]
Electric motor, engine	HEV	2020	[29]
Battery, fuel cell, fuel reformer	FCEV	2020	[30]
Battery, electric motor, fuel cell	FCEV	2020	[31]
Battery, engine, super-capacitor	HEV	2020	[32]
Fuel cell, super-capacitor	FCEV	2020	[33]

on component sizing of hybrid electric vehicle were organized [18–33]. The type of the vehicle was designated as HEV, fuel cell electric vehicle (FCEV), and electric vehicle with hybrid energy storage system (HESSEV).

Especially, studies on series HEV powertrain sizing, the characteristics of the traction motor were not adequately reflected in design and simulation. The efficiency maps of the traction motors in [34–36] were simply scaled according to the changes in the traction motor sizes. Moreover, the efficiency range of the traction motor in [35] seems to be inconsistent with that of recent technology. The minimum efficiency value was 55% and the average value was less than 80%, which do not match those observed for recent technology. In addition, in [36], the gear ratio was determined after the traction motor specifications were selected. The resultant performance thus varied according to gear ratio.

This research suggested a fuel economy optimization of heavy-duty series HEV considering traction motor characteristics. The suggested process consisted of three steps: design, modeling and simulation, and optimization, as shown in Fig. 1. The determination of the required specifications is first explained. This step presents the driving condition with the actual terrain that was considered. In step 2, the vehicle simulation construction is introduced. The modeling of the traction motor, battery, and the engine is described. Moreover, to simulate the series HEV more accurately, the process for consideration of the weight was developed. In step 3, the optimization process is demonstrated using Gaussian process modeling (GPM). The objective function comprised the gasoline-equivalent fuel economy, and the design variables considered were the gear ratio of the electric powertrain and ratio of the battery output power for the power source. In step 3, the vehicle simulation result for the optimum model was investigated and compared with that of the minimized total weight model.

The contributions of this study are as follows:

- Detailed and validated simulation models were adopted for the traction motor and battery.
- Stack length of the traction motor was determined to meet the required performance according to gear ratio.
- Efficiency map of the traction motor was calculated according to gear ratio.
- Weight of the traction motor and reduction gear were reflected according to gear ratio.

During the fuel economy optimization of series HEV, detailed and validated simulation models of traction motor and battery were used. In addition, the characteristics of the traction motor were well-reflected. The required torque and speed of the traction motor were changed according to the gear ratio. To consider this change, an electromagnetic two-dimensional finite element analysis (2D FEA) was conducted for the base model of the traction motor. On applying the proportional relationship between the stack length and output torque of the traction motor, the change in the efficiency map according to the output torque was considered. As a result, GPM-based fuel economy optimization was

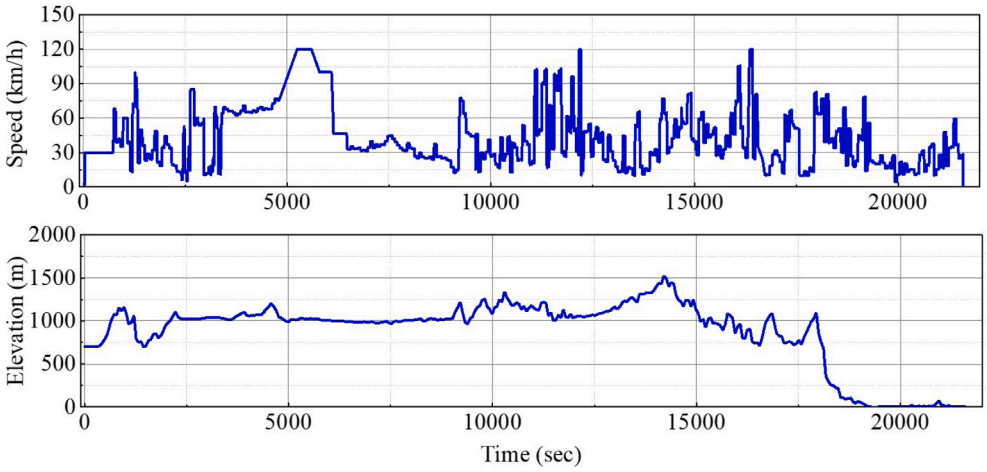

Fig. 2. Target driving cycle.

Table 2
Specifications of selected vehicle.

Items	Value	Unit
Glider weight	4300	kg
Frontal area	3.03	m^2
Overall width	2.40	m
Overall height	2.70	m
Overall length	5.40	m
Wheelbase	3.10	m
Wheel radius (include tire)	0.50	m

Table 3
Simulation conditions and information of driving cycle.

Items	Value	Unit
Air density	1.28	kg/m^3
Aerodynamic drag coefficient	0.57	–
Rolling resistance coefficient	0.01	–
Travel time	21 600	s
Travel distance	260.6	km
Maximum speed	120.00	km/h
Average speed	43.44	km/h
Maximum longitudinal slope	60.00	%
Maximum acceleration	3.42	m/s^2

conducted, considering the efficiency map and weight of the propulsion system of series HEV according to gear ratio.

2. Mathematical sizing of propulsion system considering driving condition

This section introduces the propulsion system sizing process for the series HEV. The target vehicle specifications and target driving conditions are presented. The sizing of the series hybrid propulsion system is then performed under the driving condition and a simple longitudinal vehicle dynamic equation.

2.1. Driving condition

This section explains the driving condition in addition to the target vehicle specifications, maximum speed, and maximum grade. Since the target of this study is a heavy-duty vehicle, a military tactical multi-purpose four-wheel vehicle with a diesel engine was selected [37]. This was because a tactical vehicle is generally used for a variety missions, and its powertrain can be modified for different tactical requirements. In addition, the in-wheel motor system was adopted to obtain sufficient space for the battery. Table 2 lists the selected vehicle specifications. The selected vehicle is a heavy-duty vehicle; hence, a target driving cycle was developed to include a considerable variety of vehicle speeds and altitudes. The altitude profile of this drive cycle was based on the actual terrain obtained from the randomly defined global positioning system (GPS) data path using the "GPS Route Editor" distributed by the epcian [38]. During the creation of the driving scenario, the data were tuned to prevent the consideration of unrealistic situations such as speeds that are too high or high acceleration with a high slope condition.

Table 3 presents the simulation conditions and information regarding the driving cycle. The aerodynamic drag coefficient of the *Hummer H2* was considered [39]. In addition, the maximum speed and maximum longitudinal slope were determined based on the performance

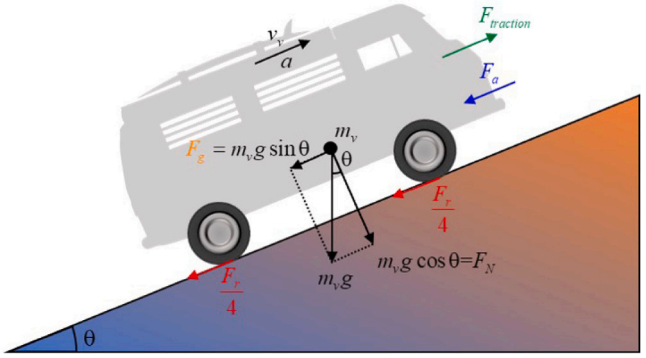

Fig. 3. Forces acting on vehicle considering longitudinal dynamics.

of existing military vehicles [40–42]. As shown in Fig. 2, the target driving cycle comprises a harsh and long mission. Because the aim of this research is mission-driven design, a driving cycle that comprises various loads with a long travel time was selected.

2.2. Propulsion system sizing

2.2.1. Electric powertrain

The driving condition consists of the airflow through the vehicle, road condition, and driving profile, elevation, speed, and acceleration. A driving scenario involving the vehicle's altitude and speed is described as a driving cycle. The driving cycle represents the trip behavior of the vehicle along the time axis, as shown in Fig. 2.

In applying simple longitudinal vehicle dynamics, the required performance of an electric powertrain can be determined based on the driving condition. Fig. 3 shows the forces acting on the vehicle. The grade resistance force F_g due to the slope, aerodynamic resistance force

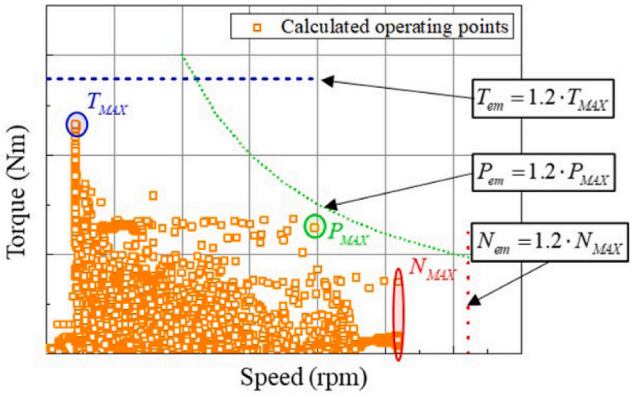

Fig. 4. Electric motor sizing considering calculated operating points.

F_a due to the airflow, and rolling resistance force F_r due to the tire contact acted on the vehicle and were expressed in equations from (1) to (3), respectively. Therein, m_v is the vehicle weight, g is the gravitational acceleration, θ is the slope angle, ρ is the air density, A_f is the frontal area of the vehicle, C_d is the drag coefficient of the vehicle, v_v is the vehicle speed, v_w is the wind speed, and f_r is the rolling resistance coefficient.

$$F_g = m_v g \sin\theta \tag{1}$$

$$F_a = \frac{1}{2}\rho A_f C_d \left(v_v + v_w\right)^2 \tag{2}$$

$$F_r = f_r m_v g \cos\theta \tag{3}$$

The traction force that the electric powertrain should deliver can be expressed using Eq. (4) if the acceleration a is given. Consequently, the corresponding requested output power P is expressed using Eq. (5).

$$F_{traction} = F_g + F_a + F_r + m_v a \tag{4}$$

$$P = F_{traction} v_v \tag{5}$$

The required torque T and the required rotational speed N from the traction motor for the drive the series HEV can be calculated using Eqs. (6) and (7), respectively, while considering that the reduction gear has the gear ratio n_g and wheel radius r_w.

$$T = \frac{r_w F_{traction}}{n_g} \tag{6}$$

$$N = n_g \frac{v_v}{r_w} \frac{60}{2\pi} \tag{7}$$

The resistance and traction forces can be calculated for the target mission using equations from (1) to (7) and the driving conditions specified in Section 2.1. Moreover, using the speed profile, these forces can be used to obtain the operating point of the traction motor. The orange squares in Fig. 4 represent the calculated operating points of each traction motor while considering the number of wheels n_w. The weight considered during this point determination was 130% of the glider weight because of the addition of the propulsion system weight.

Based on these operating points, the maximum torque of each traction motor was determined from T_{MAX} (maximum value of the calculated torque T). The maximum speed of each traction motor was also determined from N_{MAX} (maximum value of the calculated speed N). In the same manner, the maximum power of each traction motor was obtained from P_{MAX} (maximum value of the calculated power P). The peak power rating was then considered for the maximum performance curve. Therefore, even if a single operating point is on the secluded area, the traction motor should be sized to cover that point. Otherwise, the considered mission cannot be completed. As a result, the specification of each traction motor was determined using equations from (8) to (10) while considering a 20% margin to overcome losses (gear efficiency and tire slip). The determined specifications of each traction motor are as follows: torque $(T_{em}) = 4504/n_g$ N m; speed $(N_{em}) = 1000 \cdot n_g$ RPM; and output power $(P_{em}) = 126$ kW.

$$\begin{aligned} T_{em} &= 1.2 \cdot T_{MAX} \\ &= 1.2 \cdot r_w \cdot F_{traction\_MAX}/(n_w \cdot n_g) \end{aligned} \tag{8}$$

$$\begin{aligned} N_{em} &= 1.2 \cdot N_{MAX} \\ &= 1.2 \cdot n_g \cdot 60/(2\pi \cdot r_w) \cdot v_{v\_MAX} \\ &= 36 \cdot n_g \cdot v_{v\_MAX}/(\pi r_w) \end{aligned} \tag{9}$$

$$P_{em} = 1.2 \cdot P_{MAX} \tag{10}$$

2.2.2. Power source

The series HEV power source comprised an engine–generator set and battery. As expressed in Eq. (11), the gross output power of the power source should be greater than the demanded input power of the electric powertrain. η_{em}, η_{inv}, and η_{conv} represent the efficiencies of the electric motor, inverter, and converter, respectively. P_g and P_b represent the output powers of the generator and battery, respectively. η_{em} was divided to calculate the input power to the electric motor. η_{inv} and η_{conv} were multiplied while considering the loss between the transmission. In the same manner, the output power of the engine P_e was obtained by dividing P_g by the efficiency of the generator η_g, as shown in Eq. (12). Consequently, the required total output power obtained for the power source was 560 kW, and the relationship between the output power of the generator and the battery is expressed as shown in Eq. (13). The output power ratio between the battery and generator for optimizing the fuel economy of the series HEV is determined in Section 4.

$$4P_{em}/\eta_{em} = \left(P_g + P_b\right)\eta_{inv}\eta_{conv} \tag{11}$$

$$P_e = P_g/\eta_g \tag{12}$$

$$P_b + P_g = 4P_{em}/(\eta_{em}\eta_{inv}\eta_{conv}) = 560 \text{ kW} \tag{13}$$

3. Mathematical modeling of series HEV

This section introduces the mathematical model for series HEV simulation, which was performed based on an advanced vehicle simulator (ADVISOR). Fig. 5 depicts the block diagram of the series HEV simulation [43]. To secure the feasibility of the simulation result, a detailed and validated traction motor and battery model were developed and applied.

3.1. Controller modeling

In the series HEV system, the generated power from the engine–generator set is used to charge the battery, which operates the traction motor for driving. Four modes are considered for several driving environments: engine–generator alone traction mode, electric vehicle (EV) mode, and two types of hybrid traction mode (Fig. 6). The engine–generator alone traction mode drives the vehicle by using only the power generated by the engine; in contrast, the EV mode uses only the battery power. In the first hybrid mode, the vehicle is driven using the generator power, and the battery is charged when the battery SOC is less than 0.8, and there exists supplement power from the generator. In the second hybrid mode, the vehicle is driven using not only the battery power but also the generator power.

A rule-based control strategy was developed using these four driving modes. Fig. 7 presents a flow chart of the control strategy. The driving mode was determined based on the state of charge (SOC) when the

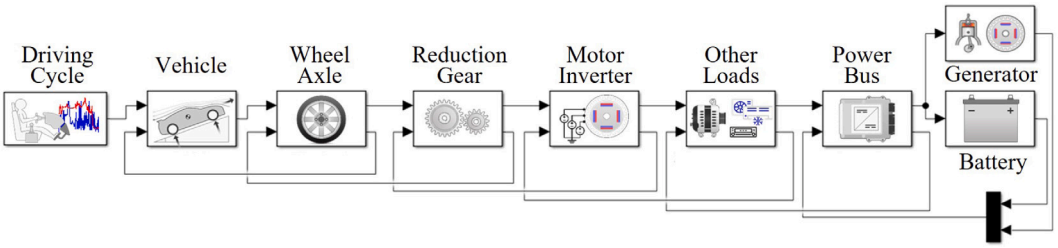

Fig. 5. Series HEV model for vehicle simulation.

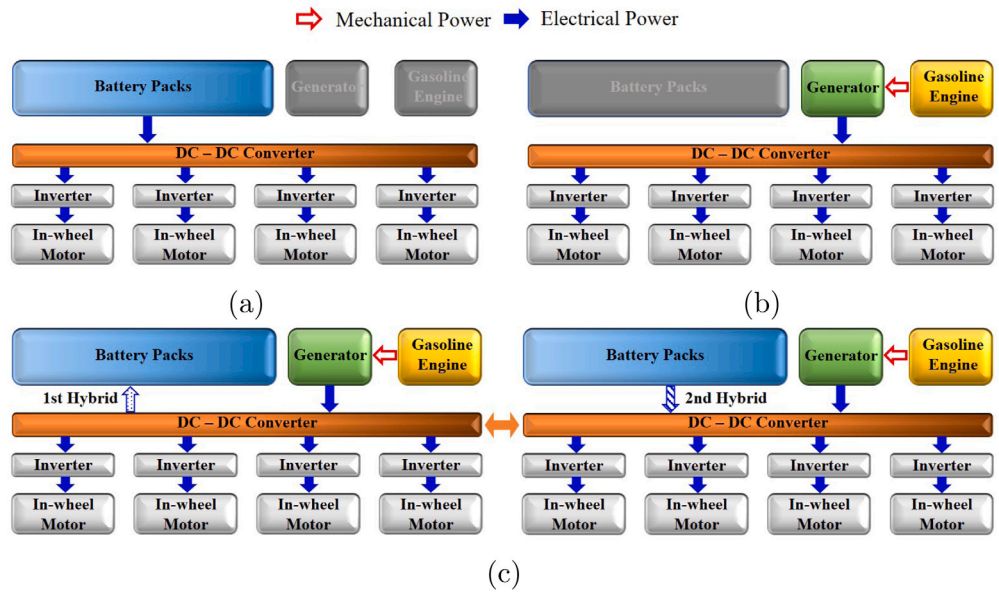

Fig. 6. Series HEV power flow and drive modes (a) EV traction mode, (b) engine–generator alone traction mode, and (c) hybrid traction mode.

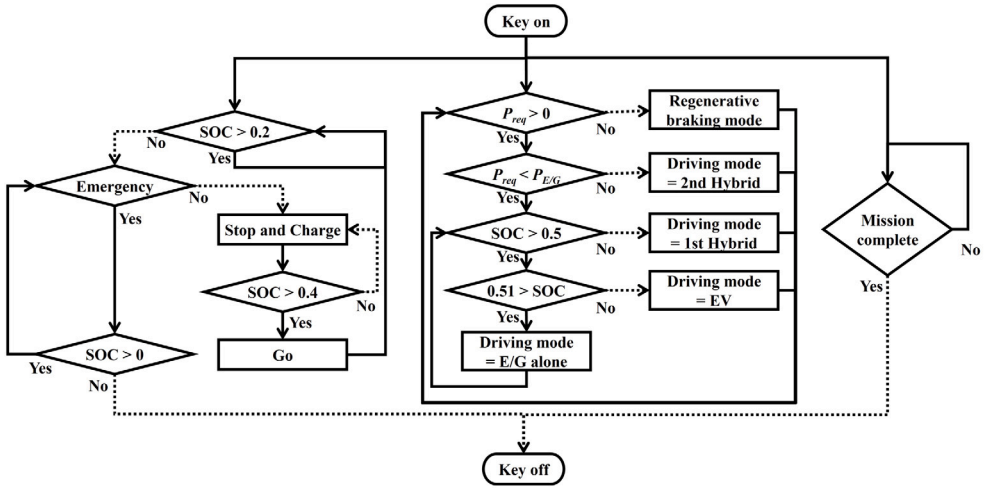

Fig. 7. Flow chart of control strategy.

required power was less than the maximum generator output power. The engine–generator alone mode was activated when the SOC was between 0.5 and 0.51. The EV mode was activated when the SOC was over 0.5, and the first hybrid mode was activated when the SOC was under 0.5. The second hybrid mode was activated when the required power was greater than the maximum generator output power. In this control strategy, an attempt is made to maintain the battery SOC at 0.5 unless the high-power demand lasts for an extended period of time. The thresholds 0.2 and 0.4 were determined to prevent the over-discharge of the battery except the emergency. And the threshold 0.5 was determined to secure the EV mode driving range. Therefore, EV mode is available in both regulatory and tactical terms.

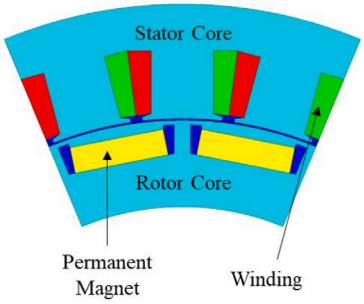

Fig. 8. Shape of base model for traction motor.

Table 4
Specification of base model of traction motor.

Items	Value	Unit
Maximum power	126	kW
Maximum speed	5000	rpm
Base speed	1000	rpm
Maximum torque (@ base speed)	1000	N m
Stack length	100	mm
Weight	110	kg
DC link voltage	620	V

3.2. Propulsion system modeling

This section presents the developed simulation model of the propulsion system. The relationships between the weights of the components and the design variables are also explained.

3.2.1. Electric powertrain

The traction motor model was constructed based on a 2D FEA. The d–q equivalent circuit was adopted to generate the efficiency map. The traction motor efficiency can be obtained using voltage equations, torque equation and losses calculation. Eq. (14) presents the voltage equations of the d and q axes of the traction motor, where R_I is the equivalent iron loss resistance, v_d is the d-axis voltage, and v_q is the q-axis voltage. v_{od} and v_{oq} are the induced voltage of the d and q axes, respectively, while ω and Ψ_a indicate the electrical rotational angular speed and the armature linkage flux, respectively. i_d and i_q are the armature currents of the d and q axes, respectively. i_{od} and i_{oq} are the iron loss subtracted values of the d- and q-axis current, respectively, which were obtained from the equivalent iron loss resistance [44].

$$\begin{bmatrix} v_d \\ v_q \end{bmatrix} = R_a \begin{bmatrix} i_{od} \\ i_{oq} \end{bmatrix} + \left(1 + \frac{R_a}{R_I}\right) \begin{bmatrix} v_{od} \\ v_{oq} \end{bmatrix} + p \begin{bmatrix} L_d & 0 \\ 0 & L_q \end{bmatrix} \begin{bmatrix} i_{od} \\ i_{oq} \end{bmatrix}$$
$$\begin{bmatrix} v_{od} \\ v_{oq} \end{bmatrix} = \begin{bmatrix} 0 & -\omega L_q \\ \omega L_d & 0 \end{bmatrix} \begin{bmatrix} i_d \\ i_q \end{bmatrix} + \begin{bmatrix} 0 \\ \omega \Psi_a \end{bmatrix} \tag{14}$$

Finally, the traction motor efficiency was calculated using equations from (15) to (17). Eq. (15) presents the output torque, where P_p is the pole pair number of the traction motor. The copper loss from the armature is expressed in Eq. (16). The traction motor efficiency can be calculated using Eq. (17) from the relationship between the input and output power [45].

$$T = P_p \left\{ \Psi_a i_{oq} + \left(L_d - L_q\right) i_{od} i_{oq} \right\} \tag{15}$$

$$W_C = R_a \left(i_d^2 + i_q^2 \right) \tag{16}$$

$$\eta_{em} = \omega_m T / (\omega_m T + W_C + W_I) \tag{17}$$

In this procedure, the base model of the traction motor was used as shown in Fig. 8. The corresponding specifications were listed in Table 4.

Table 5
Specification of base model of reduction gear.

Items	Value	Unit
Gear type	Planetary	–
Gear ratio	10:1	–
Maximum allowable output torque	3700	N m
Weight	114.5	kg

Referred from SHIMPO "VRT-285 Series Specification", official website.

Table 6
Specification of battery.

Items		Value	Unit
Nominal capacity (per cell)		2.5	Ah
Nominal voltage (per cell)		3.5	V
Weight (per cell)		0.07	kg
Maximum C-rate	Discharge	5	C
	Charge	2	C

With this base model of the traction motor, the adopted motor modeling process was validated. This procedure was conducted by using the experiment, and the overall process is illustrated in Fig. 9.

The stack length $Lstk_{em}$ of traction motor was determined according to Eq. (18). Here, T_{em_base} and $Lstk_{em\_base}$ are the maximum torque and stack length of the base model, respectively. This equation came from the relationship that the output torque of the electric motor is proportional to stack length [46,47]. In addition, the cross-sectional area of the traction motor was fixed as constant. Therefore, the weight of the traction motor is proportional to the stack length. Accordingly, the weight of the traction motor was calculated as Eq. (19), where the m_{em_base} is the weight of the base model.

$$Lstk_{em} = \frac{T_{em}}{T_{em\_base}} Lstk_{em\_base} \tag{18}$$

$$m_{em} = \frac{T_{em}}{T_{em\_base}} m_{em\_base} \tag{19}$$

For the reduction gear, a planetary type was adopted as the base model. Table 5 presents the gear specifications. A mass factor that indicates relative gear weight according to the gear ratio, was adopted. It is expressed as Eq. (20), where n_P is the planet number. Using this mass factor, the gear weight m_g was derived as shown in Eq. (21), where m_{g_base} is the base model weight [48,49].

$$f_{g\_mass} = \frac{1}{n_P} + \frac{1}{n_P\left(\frac{n_g-2}{2}\right)} + \left(\frac{n_g-2}{2}\right) + \left(\frac{n_g-2}{2}\right)^2 + \frac{0.4\left(n_g-1\right)^2}{n_P\left(\frac{n_g-2}{2}\right)} \tag{20}$$

$$m_g = \frac{f_{g\_mass}|_{n_g=n_g}}{f_{g\_mass}|_{n_g=n_{g\_base}}} m_{g\_base} \tag{21}$$

3.2.2. Power source

The type of battery was adopted as lithium-ion-type. Table 6 lists the battery specifications. A second-order resistor–capacitor (R–C) equivalent battery model was adopted for the simulation. This battery model allows us to consider the charging–discharging characteristics that occur during driving. Fig. 10 depicts the battery model and the corresponding parameters [50,51]. In addition, Coulomb counting was adopted for the SOC calculation. Although this calculation does not take into consideration the degradation of the battery, there is no problem in relative fuel economy comparison study [52,53].

In the case of the generator for the engine–generator of the series HEV, the operating speed of the generator is totally decoupled from the vehicle speed. Therefore, the generator is usually operated at the most efficient point. As a result, the efficiency was assumed to be 95%

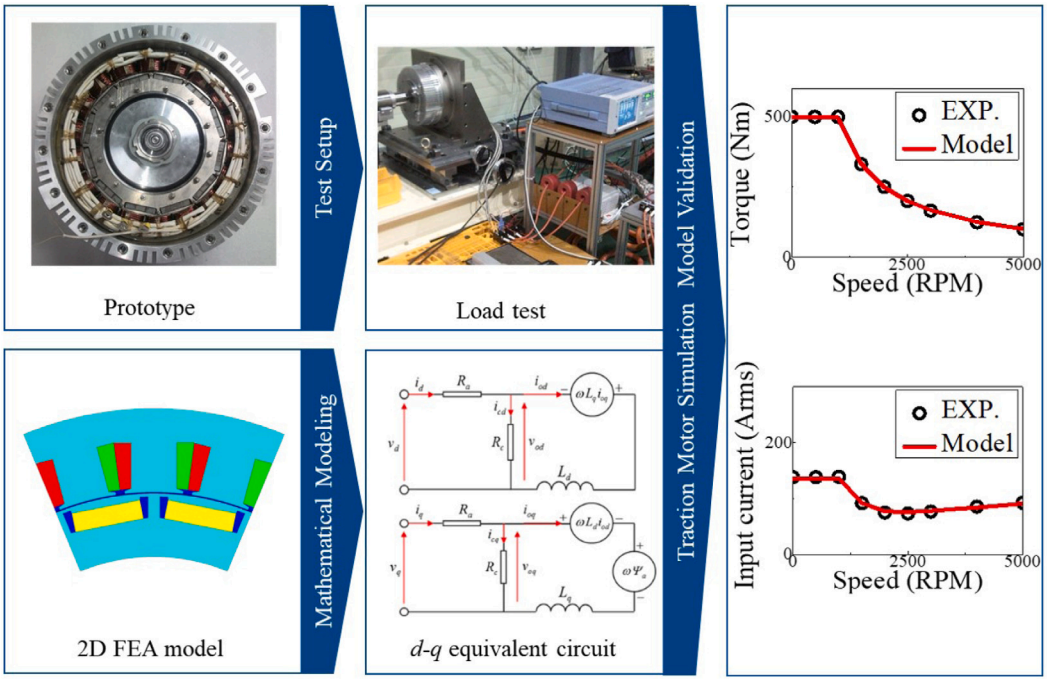

Fig. 9. Validated electric motor model.

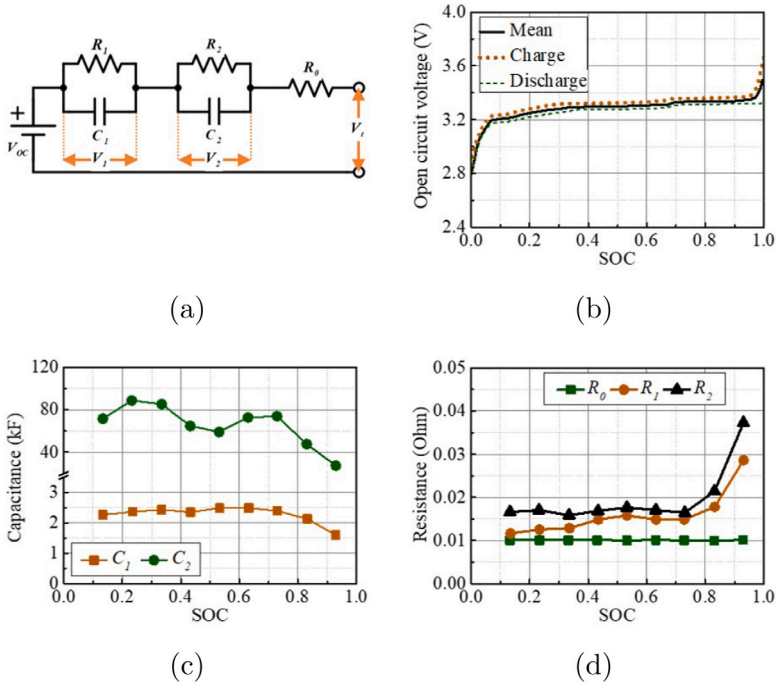

Fig. 10. Second-order R–C equivalent model and corresponding parameters of battery for vehicle simulation.

while considering an efficient operation. Herein, to consider the real condition of an engine–generator set, the efficiency map of a gasoline engine was adopted for the generator (Fig. 11) [54]. This efficiency map was scaled and used for all the design points.

The weight of the generator and battery were also formulated. The weight per cell for the battery was known; therefore, the weight could be calculated if the number of cells was determined according to the output power. The number of cells n_{cell} is expressed, as shown in Eq. (22), where V_{nom} is the nominal voltage, Ah_{nom} is the nominal capacity, and C_{MAX} is the maximum discharge rate. The battery weight m_b is expressed, as shown in Eq. (23). The power-to-weight ratio for the generator was assumed to be 1.5 kW/kg; thus, the weight was directly calculated according to the output power. Several engine specifications for commercial vehicles were referred to for the engine of the generator. Fig. 12 depicts the power versus weight curve. The engine weight was considered based on this curve.

$$n_{cell} = \frac{P_b}{V_{nom} Ah_{nom} C_{MAX}} = \frac{P_b}{43.75} \tag{22}$$

$$m_b = 0.07 \cdot n_{cell} \tag{23}$$

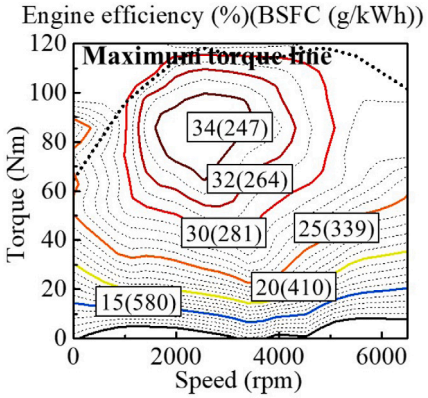

Fig. 11. Gasoline engine efficiency map for generator.

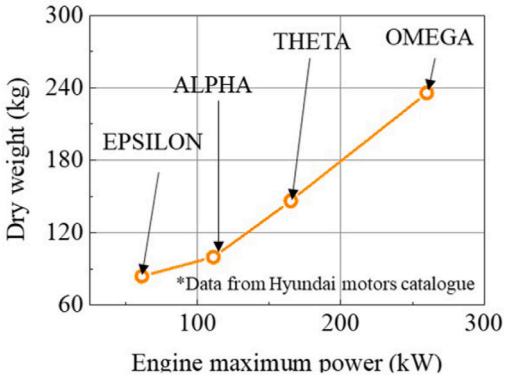

Fig. 12. Gasoline engine weight versus power curve.

4. GPM-based fuel economy optimization

This section presents the surrogate model-based optimization of the fuel economy of the series HEV. The developed design process and the simulation model presented in Sections 2 and 3 are used. Optimal Latin hypercube design (OLHD) was adopted in the design of experiment (DOE) stage. The surrogate model was then generated using a GPM.

4.1. Optimum design formulation

The design problem formulation should be performed in advance for optimization. The design variables were the weights and specifications of the electric powertrain and the power source, gear ratio, and the proportion of the generator output power and battery output power. The electric powertrain specifications were determined (wheel torque and wheel speed), as mentioned in Section 2. In addition, the weight relationship of the electric powertrain according to the gear ratio, was also formulated. Moreover, the overall specifications of the power sources were determined in Section 3. Therefore, the power source weights can be calculated according to the output power proportions of the generator and battery. Consequently, the design variables were determined to be the gear ratio and the output power ratio between the generator and the battery. In summary, the optimum design problem formulation could be performed as follows. Here, f denotes fuel economy of series HEV, h_1 denotes total power of the source (battery and engine/generator), h_2 denotes the maximum wheel speed, h_3 denotes the maximum wheel torque, and g denotes the driving cycle trace error. The design variables x_1 and x_2 are gear ratio and battery proportion, respectively.

Objective function : maximize $f(\mathbf{x})$

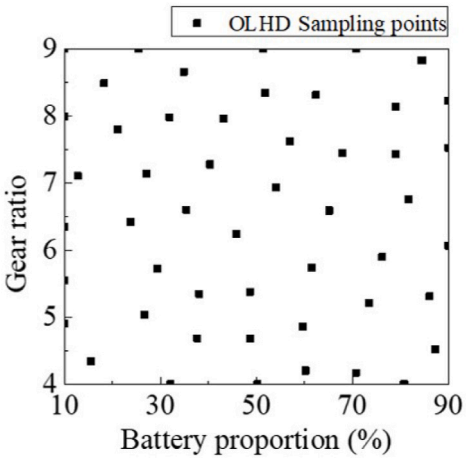

Fig. 13. Optimal Latin hypercube design results for two design variables: gear ratio and battery proportion.

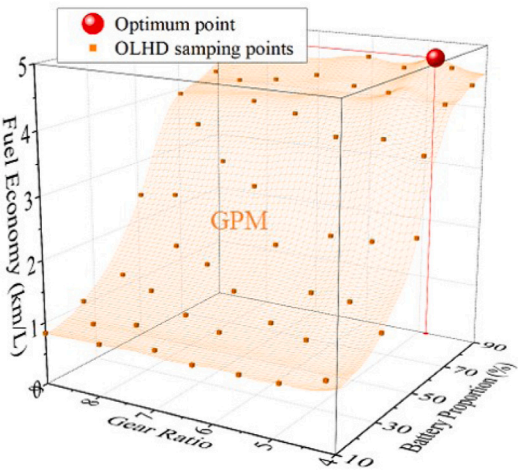

Fig. 14. Surrogate modeling result of fuel economy of series HEV.

Design variables : x_1, x_2

Subjected to

Equality constraints : $h_1(\mathbf{x}) = 560,\ h_2(\mathbf{x}) = 1000,\ h_3(\mathbf{x}) = 4507$

Inequality constraint : $g(\mathbf{x}) \leq 1$

Variable bounds : $4 \leq x_1 \leq 9,\ 10 \leq x_2 \leq 90$

4.2. Surrogate model generation

In this section, the surrogate model of fuel economy was constructed from GPM. First, the DOE was performed using OLHD. The reason of the characteristics of the Latin hypercube design (LHD) generates the non-collapsing sampling points [55,56]. Moreover, the maximum distance between the sampling points was maximized. The OLHD sampling result is shown in Fig. 13. Then the series HEVs were modeled for the sampling points to perform fuel economy simulation. During the simulation, the stack length, efficiency map of the traction motor, according to the gear ratio, were considered. In addition, the weight of the power sources was reflected according to the battery proportion.

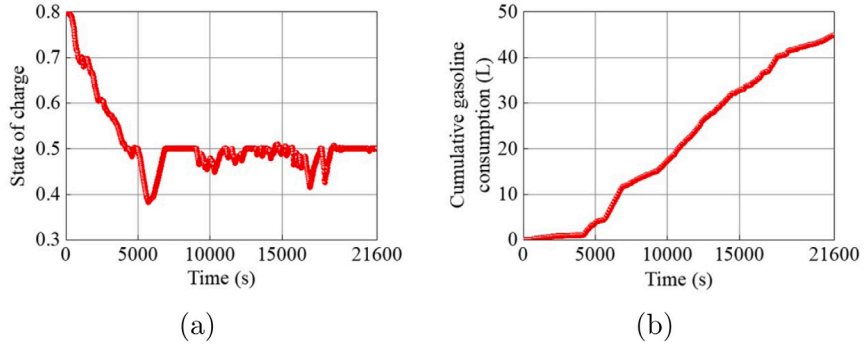

Fig. 15. Energy usage profile during vehicle simulation for optimum model: (a) battery SOC and (b) gasoline consumption.

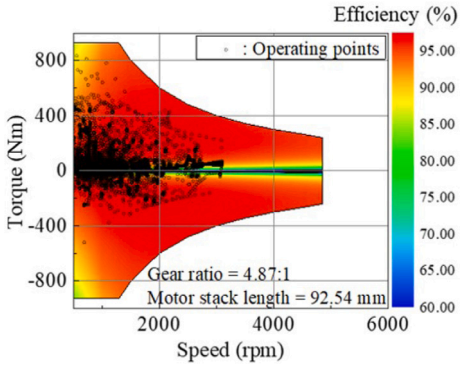

Fig. 16. Efficiency map of traction motor and operating points of traction motor from vehicle simulation for optimum model.

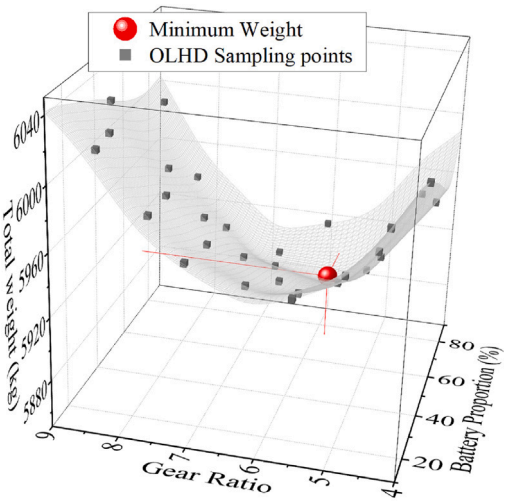

Fig. 17. Surrogate modeling result of total weight of series HEV.

Finally, the gasoline-equivalent fuel economy explained in Eq. (24) was calculated from the vehicle simulation while considering the battery consumption.

$$\text{Gasoline } 1.13 = 8.9 \text{ kWh} \tag{24}$$

Based on the vehicle simulation results, the fuel economy surrogate model was constructed by using GPM. The constructed fuel economy surrogate model is shown in Fig. 14. However, to secure the reliability of the optimization result, the accuracy of the surrogate model should be verified. This study adopted the leave-one-out cross-validation method [57]. The normalized root-mean-square error (NRMSE) of the fuel economy surrogate model from GPM was defined as Eq. (25). Here, n_s is the number of sample points, $\mathbf{x}$ is the vector of design variables, $\mathbf{Y}(\mathbf{x})$ is the response i.e. fuel economy from vehicle simulation, x_i is the value of the design variables at the ith sample point, $Y(x_i)$ is the response of the ith sample point from vehicle simulation, and $\hat{Y}^{(-i)}(x_i)$ is the predicted response of the ith sample point from the GPM surrogate model except for the ith sample point. The leave-one-out cross-validation result is 3.28%. This result shows that the constructed fuel economy surrogate model has sufficient accuracy to be used in optimization.

$$\text{NRMSE} = \sqrt{\frac{1}{n_s}\sum_{i=1}^{n_s}\left(\frac{Y(x_i) - \hat{Y}^{(-i)}(x_i)}{\max\{\mathbf{Y}(\mathbf{x})\} - \min\{\mathbf{Y}(\mathbf{x})\}}\right)^2} \cdot 100\% \tag{25}$$

4.3. Fuel economy optimization

The surrogate model of the fuel economy was generated, as shown in Fig. 14. The orange mesh surface represents the surrogate model from the GPM, while the orange cube represents the experiment points obtained from the OLHD. Using the fuel economy surrogate model, the fuel economy optimization was conducted using the steepest gradient descent algorithm. The red ball in Fig. 14. denotes the optimum design point of the fuel economy. The expected fuel economy of optimum series HEV was 4.73 km/L.

5. Results

5.1. Fuel economy optimization result

The design results obtained using the suggested process with GPM are listed in Table 7. The reduction gear ratio was determined as 4.87:1, and the output power ratio between the battery and generator was determined as 89.8:10.2. The expected gasoline-equivalent fuel economy, including the battery consumption, was 4.73 km/L. To validate the design results, vehicle simulation was conducted. The verification result of the fuel economy optimization is listed in Table 8. The error between the simulation and estimated results is 0.85% for the optimum design point.

To investigate the design results, the battery SOC profiles and cumulative gasoline consumption profiles were depicted, as shown in Fig. 15. In addition, with respect to the traction motor design result, the efficiency map and operating points are depicted in Fig. 16. The efficiency maps were generated from the validated model while considering the determined gear ratio.

5.2. Additional study : Weight minimization

The vehicle weight minimization was performed according to the suggested process, in terms of performance maximization. The design

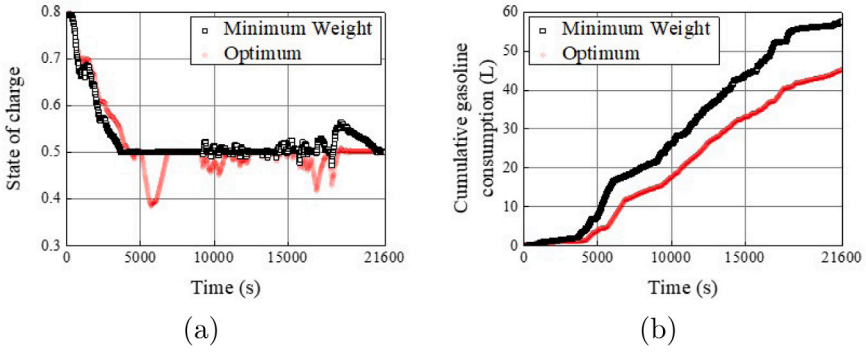

Fig. 18. Comparison of energy usage profile during vehicle simulation for fuel economy optimum and weight minimum model: (a) battery SOC and (b) gasoline consumption.

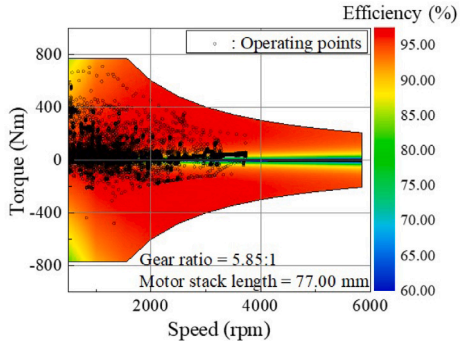

Fig. 19. Efficiency map of traction motor and operating points of traction motor from vehicle simulation for weight minimum model.

Table 7
Design result from suggested sizing and optimization process.

Items		Value	Unit
Glider weight		4300	kg
Traction motor	Output power (4ea)	504	kW
	Stack length (1ea)	92.5	mm
	Armature resistance (1ea)	38.1	mΩ
	Base speed (1ea)	1300	rpm
	Maximum speed (1ea)	4870	rpm
	Maximum torque (1ea)	925.4	N m
	Weight (4ea)	407.2	kg
Reduction gear	Gear ratio (1ea)	4.87:1	–
	Weight (4ea)	97.1	kg
Battery	Output power[a]	502.7	kW
	Weigh[b]	854.3	kg
Generator	Output power	57.3	kW
	Weigh	38.2	kg
Engine	Output power	63.7	kW
	Weigh	89.2	kg
Battery output power: Generator output power		89.8:10.2	–
Power electronics devices weight		150	kg
Overall vehicle weight		5936	kg

[a]At 5 C discharge rate.
[b]Weight of packaging was assumed as 50 kg.

result is organized in Table 9. The result was the stack length of the electric motor was decreased, the gear ratio was increased, and the proportion of the battery was decreased compared to the fuel economy optimum model. To perform this optimization, the GPM of the total weight, which is shown in Fig. 17, was used. This optimization resulted in 44 kg total weight decrease. Therefore, the acceleration performance was improved compared to the fuel economy optimum model. The comparison results are organized in Table 10.

Table 8
Validation result of fuel economy surrogate modeling.

Model	Fuel economy (km/L)		Error (%)
	Estimated from GPM	Vehicle simulation	
Optimum	4.73	4.69	0.85

Table 9
Weight minimization result.

Items	Value	Unit
Traction motor stack length	77.0	mm
Reduction gear ratio	5.85:1	–
Battery output power: Generator output power	74.7:25.3	–
Overall vehicle weight	5892	kg

Table 10
Acceleration performance simulation results.

Model	Acceleration time (s)		
	0–100 km/h	60–100 km/h	0–120 km/h
Weight minimum	9.50	5.60	13.70
Optimum	9.54	5.69	13.86

As a result of the weight minimization, the performance was slightly improved. However, the gasoline-equivalent fuel economy was 4.25 km/h. Compared to the fuel economy optimum model, the fuel economy was decreased by 9.4%. To inspect the situation, the SOC and cumulative gasoline consumption histories during the vehicle simulation were compared between the fuel economy optimum model and the weight minimum model. The comparison result is shown in Fig. 18. According to these graphs, the minimum weight model acted to use more gasoline instead of adequate battery use.

In addition, the investigation on the traction motor operation was performed. The efficiency map and operating points of the traction motor for the weight minimum model are shown in Fig. 19. Moreover, the comparison of the operating efficiency profile of the traction motor is depicted in Fig. 20.

Summarizing the result of Section 5.2, there is no merit of weight minimization. The acceleration performance was maximally improved by 1.1%, compared to the fuel economy optimum model. However, the fuel economy was decreased by 9.2%, compared to the fuel economy optimum model. Especially, 60–100 km, which affects the sense of acceleration, was only increased 0.4%, compared to the fuel economy optimum model. Therefore, the availability of the suggested sizing and optimization process for the HEV powertrain design was confirmed.

6. Conclusion

In this study, the fuel economy optimization of a propulsion system for a heavy-duty series HEV was investigated. The sizing process for the propulsion system was first formulated based on simple vehicle

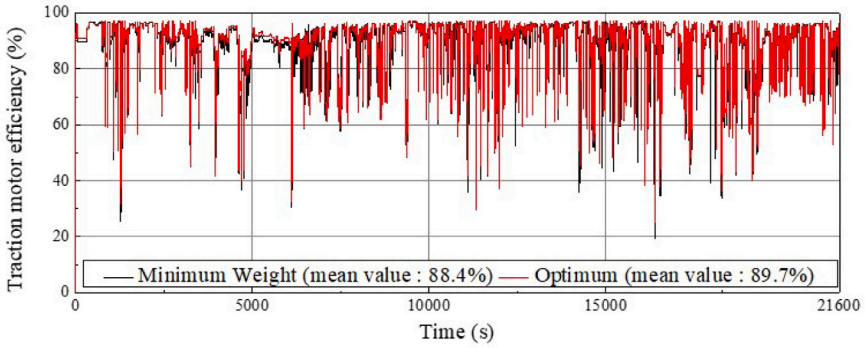

Fig. 20. Comparison of efficiency profile of traction motor for fuel economy optimum and weight minimum model.

dynamics while considering the driving conditions and specifications. The driving simulation was then developed using ADVISOR. The control strategy and the traction motor and battery models applied were developed in this study. Moreover, to appropriately perform vehicle simulation, the weight changes of each component were formulated and considered. Using the developed design and simulation process for the series HEV, fuel economy optimization was conducted. In this optimization process, GPM was adopted for the surrogate model generation. The gear ratio and battery output power proportion were selected as design variables. The fuel economy optimum point achieved was 4.73 km/L in terms of gasoline fuel economy. In addition, the fuel economy surrogate model was validated by using leave-one-out cross-validation. Furthermore, the optimization result was validated based on a comparison between the estimated from GPM and simulation results. The simulation result was 4.69 km/L, which shows a 0.85% error. Therefore, it can be concluded that the suggested fuel economy optimization process for heavy-duty series HEV from this study has effectiveness.

CRediT authorship contribution statement

Dong-Min Kim: Conceptualization, Methodology, Writing – original draft. **Soo-Gyung Lee:** Validation, Formal analysis. **Dae-Kee Kim:** Investigation, Resources. **Min-Ro Park:** Writing – review & editing. **Myung-Seop Lim:** Supervision.

Declaration of competing interest

The authors declare that they have no known competing financial interests or personal relationships that could have appeared to influence the work reported in this paper.

References

[1] Roychowdhury A, Nasim U. Trucks: Heavy-duty pollution and action. New Delhi: Centre for Science and Environment; 2016.
[2] Dennis B. EPA to weigh tougher pollution standards for heavy-duty trucks. 2018, [https://www.washingtonpost.com/energy-environment/2018/11/13/epa-toughen-pollution-standards-heavy-duty-trucks/] (accessed on March 9, 2022).
[3] Çabukoglu E, Georges G, Küng L, Pareschi G, Boulouchos K. Battery electric propulsion: An option for heavy-duty vehicles? Results from a Swiss case-study. Transp Res C 2018;88:107–23.
[4] Naumanen M, Uusitalo T, Huttunen-Saarivirta E, van der Have R. Development strategies for heavy duty electric battery vehicles: Comparison between China, EU, Japan and USA. Resour Conserv Recy 2019;151:104413.
[5] Liimatainen H, van Vliet O, Aplyn D. The potential of electric trucks – An international commodity-level analysis. Appl Energy 2019;236:804–14.
[6] Wu Y, Wang W, Ming J, Li M, Xie L, He X, Wang J, Liang S, Wu Y. An exploration of new energy storage system: High energy density, high safety, and fast charging lithium ion battery. Adv Funct Mater 2019;29.
[7] Somà A. Trends and hybridization factor for heavy-duty working vehicles. In: Donateo T, editor. Hybrid electric vehicles. Rijeka: IntechOpen; 2017, http://dx.doi.org/10.5772/intechopen.68296.
[8] Gu J, Zhao Z, Chen Y, He L, Zhan X. Integrated optimal design of configuration and parameter of multimode hybrid powertrain system with two planetary gears. Mech Mach Theory 2020;143:103630.
[9] Cammalleri M, Castellano A. Analysis of hybrid vehicle transmissions with any number of modes and planetary gearing: kinematics, power flows, mechanical power losses. Mech Mach Theory 2021;162:104350.
[10] Liu T, Hu X, Li SE, Cao D. Reinforcement learning optimized look-ahead energy management of a parallel hybrid electric vehicle. IEEE/ASME Trans Mechatronics 2017;22(4):1497–507.
[11] Mamun A-A, Liu Z, Rizzo DM, Onori S. An integrated design and control optimization framework for hybrid military vehicle using lithium-ion battery and supercapacitor as energy storage devices. IEEE Trans Transp Electrif 2019;5(1):239–51.
[12] Khan MMS, Faruque MO, Newaz A. Fuzzy logic based energy storage management system for MVDC power system of all electric ship. IEEE Trans Energy Convers 2017;32(2):798–809.
[13] Zhu H, Song Z, Hou J, Hofmann HF, Sun J. Simultaneous identification and control using active signal injection for series hybrid electric vehicles based on dynamic programming. IEEE Trans Transp Electrif 2020;6(1):298–307.
[14] Tang X, Chen J, Liu T, Qin Y, Cao D. Distributed deep reinforcement learning-based energy and emission management strategy for hybrid electric vehicles. IEEE Trans Veh Technol 2021;70(10):9922–34.
[15] Tang X, Chen J, Pu H, Liu T, Khajepour A. Double deep reinforcement learning-based energy management for a parallel hybrid electric vehicle with engine start-stop strategy. IEEE Trans Transp Electrif 2021;Early Access:1.
[16] Ehsani M, Gao Y, Longo S, Ebrahimi K. Modern electric, hybrid electric, and fuel cell vehicles. Boca Raton: CRC Press/Taylor & Francis Group; 2019.
[17] Li Y, Tang X, Lin X, Grzesiak L, Hu X. The role and application of convex modeling and optimization in electrified vehicles. Renew Sustain Energy Rev 2022;153:111796.
[18] Li J, Wang H, He H, Wei Z, Yang Q, Igic P. Battery optimal sizing under a synergistic framework with DQN based power managements for the fuel cell hybrid powertrain. IEEE Trans Transp Electrif 2021;1.
[19] Mahmoodi-k M, Montazeri M, Madanipour V. Simultaneous multi-objective optimization of a PHEV power management system and component sizing in real world traffic condition. Energy 2021;233:121111.
[20] Li M, Wang L, Wang Y, Chen Z. Sizing optimization and energy management strategy for hybrid energy storage system using multiobjective optimization and random forests. IEEE Trans Power Electron 2021;36(10):11421–30.
[21] Taghavifar H. Fuel cell hybrid range-extender vehicle sizing: Parametric power optimization. Energy 2021;229:120786.
[22] Shaobo X, Qiankun Z, Xiaosong H, Yonggang L, Xianke L. Battery sizing for plug-in hybrid electric buses considering variable route lengths. Energy 2021;226:120368.
[23] Kabalan B, vinot e, Trigui R, Dumand C. Designing hybrid vehicle architectures: Utilizing an automatic generation and optimization approach. IEEE Veh Technol Mag 2021;16(2):76–85.
[24] Yu H, Castelli-Dezza F, Cheli F, Tang X, Hu X, Lin X. Dimensioning and power management of hybrid energy storage systems for electric vehicles with multiple optimization criteria. IEEE Trans Power Electron 2021;36(5):5545–56.
[25] Zhu T, Wills RG, Lot R, Kong X, Yan X. Optimal sizing and sensitivity analysis of a battery-supercapacitor energy storage system for electric vehicles. Energy 2021;221:119851.
[26] da Silva SF, Eckert JJ, Silva FL, Silva LC, Dedini FG. Multi-objective optimization design and control of plug-in hybrid electric vehicle powertrain for minimization of energy consumption, exhaust emissions and battery degradation. Energy Convers Manage 2021;234:113909.
[27] Molina S, Novella R, Pla B, Lopez-Juarez M. Optimization and sizing of a fuel cell range extender vehicle for passenger car applications in driving cycle conditions. Appl Energy 2021;285:116469.

[28] Zhang L, Ye X, Xia X, Barzegar F. A real-time energy management and speed controller for an electric vehicle powered by a hybrid energy storage system. IEEE Trans Ind Inf 2020;16(10):6272–80.
[29] Anselma PG, Niutta CB, Mainini L, Belingardi G. Multidisciplinary design optimization for hybrid electric vehicles: component sizing and multi-fidelity frontal crashworthiness. Struct Multidiscip Optim 2020;62(4):2149–66.
[30] Purnima P, Jayanti S. Optimal sizing of a fuel processor for auxiliary power applications of a fuel cell-powered passenger car. Int J Hydrogen Energy 2020;45(48):26005–19.
[31] Hou S, Gao J, Zhang Y, Chen M, Shi J, Chen H. A comparison study of battery size optimization and an energy management strategy for FCHEVs based on dynamic programming and convex programming. Int J Hydrogen Energy 2020;45(41):21858–72.
[32] He Y, Wang C, Zhou Q, Li J, Makridis M, Williams H, Lu G, Xu H. Multiobjective component sizing of a hybrid ethanol-electric vehicle propulsion system. Appl Energy 2020;266:114843.
[33] Gaikwad SD, Ghosh PC. Sizing of a fuel cell electric vehicle: A pinch analysis-based approach. Int J Hydrogen Energy 2020;45(15):8985–93.
[34] Borthakur S, Subramanian SC. Design and optimization of a modified series hybrid electric vehicle powertrain. Proc Inst Mech Eng D 2019;233(6):1419–35.
[35] Zhang L, Liu W, Qi B. Innovation design and optimization management of a new drive system for plug-in hybrid electric vehicles. Energy 2019;186.
[36] Arıkan FR. Sizing of a series hybrid electric vehicle (Master's thesis), Middle East Technical University; 2019.
[37] MorozovKMDB. DOZOR-B armoured personnel carrier. 2021, [http://morozov.com.ua/en/bronetankovaya-tehnika-i-vooruzhenie/boevye-bronirovannye-mashiny/razrabotki/dozor-b/] (accessed on March 9, 2022).
[38] GpsNoteNET. GPS route editor. 2021, [http://www.gpsnote.net/] (accessed on March 9, 2022).
[39] Dumas L. CFD-based optimization for automotive aerodynamics. In: Thévenin D, Janiga G, editors. Optimization and computational fluid dynamics. Berlin: Springer; 2008.
[40] Rizzo DM. Military vehicle optimization and control (Ph.D. thesis), Michigan Technological University; 2014.
[41] Kramer DM, Parker GG. Current state of military hybrid vehicle development. Int J Electr Hybrid Veh 2011;3(4):369–87.
[42] MILITARY TODAY - Everything about modern warfare. 2021, [http://www.military-today.com/] (accessed on March 9, 2022).
[43] Markel T, Brooker A, Hendricks T, Johnson V, Kelly K, Kramer B, O'Keefe M, Sprik S, Wipke K. ADVISOR: a systems analysis tool for advanced vehicle modeling. J Power Sources 2002;110(2):255–66.
[44] Kim D-M, Chin J-W, Hong J-P, Lim M-S. Performance prediction of surface-mounted permanent magnet synchronous motor based on ring specimen test result. IET Electr Power Appl 2019;13(9):1280–6.
[45] Lim M-S, Chai S-H, Yang J-S, Hong J-P. Design and verification of 150-krpm PMSM based on experiment results of prototype. IEEE Trans Ind Electron 2015;62(12):7827–36.
[46] Bianchi N, Jahns TM. Design, analysis, and control of interior pm synchronous machines: Presented at the IEEE industry applications society annual meeting Seattle, USA, October 3rd, 2004. Padova: CLEUP; 2006.
[47] Kim H-J, Jeong J-S, Yoon M-H, Moon J-W, Hong J-P. Simple size determination of permanent-magnet synchronous machines. IEEE Trans Ind Electron 2017;64(10):7972–83.
[48] Roos F, Spiegelberg C. Relations between size and gear ratio in spur and planetary gear trains. Stockholm: KTH; 2005.
[49] Rejman E, Rejman M. Gears weight equations - gear chain weight calculation methodology. Mach Technol Mater 2011;5(2):18–21, [https://mech-ing.com/journal/Archive/2011/2/22_E.Rejman,%20M.Rejman.pdf].
[50] Perez HE. Model based optimal control, estimation, and validation of lithium-ion batteries (Ph.D. thesis), Berkeley: University of California; 2016.
[51] Klein M, Tong S, Park J. In-plane nonuniform temperature effects on the performance of a large-format lithium-ion pouch cell. Appl Energy 2016;165:639–47.
[52] He J, Wei Z, Bian X, Yan F. State-of-health estimation of lithium-ion batteries using incremental capacity analysis based on voltage–capacity model. IEEE Trans Transp Electrif 2020;6(2):417–26.
[53] Goud JS, R K, Singh B. An online method of estimating state of health of a li-ion battery. IEEE Trans Energy Convers 2021;36(1):111–9.
[54] Reilly DJ, Andersen RP, Casparian RJ, Dugdale PH. Saturn DOHC and SOHC four cylinder engines. In: International congress & exposition. SAE International; 1991.
[55] Sacks J, Welch WJ, Mitchell TJ, Wynn HP. Design and analysis of computer experiments. Statist Sci 1989;4(4):409–23.
[56] Lee S-G, Kim S, Park J-C, Park M-R, Lee TH, Lim M-S. Robust design optimization of SPMSM for robotic actuator considering assembly imperfection of segmented stator core. IEEE Trans Energy Convers 2020;35(4):2076–85.
[57] Queipo NV, Haftka RT, Shyy W, Goel T, Vaidyanathan R, Kevin Tucker P. Surrogate-based analysis and optimization. Prog Aerosp Sci 2005;41(1):1–28.